Mesoporous $W_{18}O_{49}$ Hollow Spheres as Highly Active Photocatalyst

Zhen-Feng Huang†, Jiajia Song†, Lun Pan†, Fenglei Lv†, Qingfa Wang†, Ji-Jun Zou*†‡, Xiangwen Zhang†‡, and Li Wang†‡

†Key Laboratory for Green Chemical Technology of the Ministry of Education, School of Chemical Engineering and Technology, Tianjin University, Tianjin 300072, China

‡Collaborative Innovative Center of Chemical Science and Engineering (Tianjin), Tianjin 300072, China

**E-mail: jj_zou@tju.edu.cn; Fax: +86-22-27892340; Tel: +86-22-27892340.*

Table of contents

	Captions
Table S1	BET surface area of $W_{18}O_{49}$.
Fig. S1	(a-c) SEM, TEM and HRTEM images of UWS, and (d-f) SEM, TEM and HRTEM images of NWS.
Fig. S2	(a) N_2 adsorption/desorption isotherms and (b) pore distribution of HWS.
Fig. S3	W4f XPS spectra of $W_{18}O_{49}$ samples.
Fig. S4	SEM images of $W_{18}O_{49}$ after ball-milling. (a: HWS; b: UWS; c:NWS)
Fig. S5	(a) C/C_0 and TOC/TOC_0 as a function of irradiation time (t) for MO degradation, and (b) Photoreaction rates in degradation of MO under UV-vis light.
Fig. S6	Photoreaction rates in degradation of phenol under UV-vis light.
Fig. S7	Photoreaction rates before and after ball-milling in degradation of MO under visible light.
Fig. S8	Photoreaction rates of hollow and solid spheres in degradation of MO and phenol under UV-vis light.
Fig. S9.	(a, b) SEM images and (c) XRD patterns of HWS before and after photocatalytic reaction.
Fig. S10	Photocurrent density versus applied voltage in 0.2 M Na_2SO_4 aqueous under UV-vis irradiation.

Experimental Section

Materials:

WCl_6 and phenol were obtained from J&K Chemical. Acetic acid (CH_3COOH), methyl orange (MO), n-propanol and absolute ethanol (C_2H_5OH), were purchased from Tianjin Guangfu Fine Chemical Research Institute. All the reagents were reagent grade and used as received.

Material preparation:

HWS: WCl_6 (0.15 g) were dissolved in acetic acid (50 mL) and stirred for 30 min at room temperature. The solution was transferred to a Teflon-lined stainless steel autoclave (100 mL) and heated at 180 °C for 16 h. The resultant powders were separated via centrifugation, washed with high purity water and ethanol for 3 times, and finally dried at 40 °C overnight.

UWS: WCl_6 (1.6 g) were dissolved in absolute ethanol (80 mL) and stirred for 30 min at room temperature. The solution was transferred to a Teflon-lined stainless steel autoclave (100 mL) and heated at 160 °C for 24 h. The resultant powders were separated via centrifugation, washed with high purity water and ethanol for 3 times, and finally dried at 40 °C overnight.

NWS: WCl_6 (0.297 g) were dissolved in n-propanol (50 mL) and stirred for 30 min at room temperature. The solution was transferred to a Teflon-lined stainless steel autoclave (100 mL) and heated at 200 °C for 24 h. The resultant powders were separated via centrifugation, washed with high purity water and ethanol for 3 times, and finally dried at 40 °C overnight.

Photocatalytic performance tests:

The photodegradation of MO and phenol were conducted in aqueous solution vertically irradiated by a 300 W high-pressure xenon lamp (PLS-SXE-300UV, Beijing Trusttech. Co. Ltd.). The UV-vis (200-800 nm) was separated by vis-ref and UV-cut optical filters. The intensity is 37.0 $mW\cdot cm^{-2}$ at 365 nm for UV-vis light, and 43.0 $mW\cdot cm^{-2}$ at 420 nm for visible light. The irradiation area of the light source was ca. 20 cm^2. The reactor was open to air in order to reach the air-equilibrated condition. Typically, 50 mg of photocatalyst were dispersed in 50 mL MO (0.12 mM) or phenol (0.2 mM) solution with magnetic stirring. Prior to the irradiation, the suspension was stirred for 60 min in the dark to ensure the adsorption equilibrium. The reaction temperature was controlled at 25 °C with no acid or alkaline reagents added. During the reaction, materials were withdrawn at intervals, centrifuged, and analyzed. The concentration of residual was determined using a Hitachi U-3010 UV-vis spectrometer by monitoring the characteristic absorption wavelength of 463 nm for MO or 270 nm for phenol, and the data were fitted using a pseudo-first-order kinetic equation to obtain the reaction rate constant (k). In addition, the total organic carbon (TOC) of some samples was measured by a Shimadzu TOC-V_{CPH} analyzer.

Photoelectrochemical performance tests:

Photoelectrochemical tests were performed on Autolab potentiostat/galvanostat (Model PGSTAT 302N) workstation using three-electrode cell with a working electrode, a Pt counter electrode, and a Ag/AgCl reference electrode. Na_2SO_4 (0.2 M) was used as electrolyte solution. The working electrode was prepared by dip-coating photocatalyst slurry on a F-doped tin oxide (FTO) glass electrode (1 cm × 1.5 cm) and subsequently heating at 40 °C for three day. All investigated working electrodes were of similar thickness. All potentials were obtained with reference to the Ag/AgCl.

Characterization:

The crystal structures were recorded using a Rigaku D/max-2500 X-ray diffractometer (XRD) equipped with a Cu Kα irradiation source. The BET surface area was determined using N_2 adsorption/desorption isotherm measurements at -196 ºC on a Micrometrics TriStar 3000 equipment. The morphology and microstructure were examined on a Tecnai G^2 F20 transmission electron microscopy (TEM) operated at 200 kV and a Nanosem 430 field emission scanning electron microscopy (SEM). UV-vis diffuse reflectance spectra (UV-vis DRS) were recorded with a Hitachi U-3010 spectrometer equipped with a 60 mm diameter integrating sphere using $BaSO_4$ as the reference, and defined amount of powder were pressed into self-supporting thick pellet for measurement. Surface chemical states were analyzed with a PHI-1600 X-ray photoelectron spectroscope (XPS) equipped with Al Kα radiation, and the binding energy was calibrated by the C1s peak (284.6 eV) of the contamination carbon.

Material	**HWS**	**UWS**	**NWS**
BET (m^2/g)	114.4	169.2	58.4

Table S1. BET surface area of $W_{18}O_{49}$.

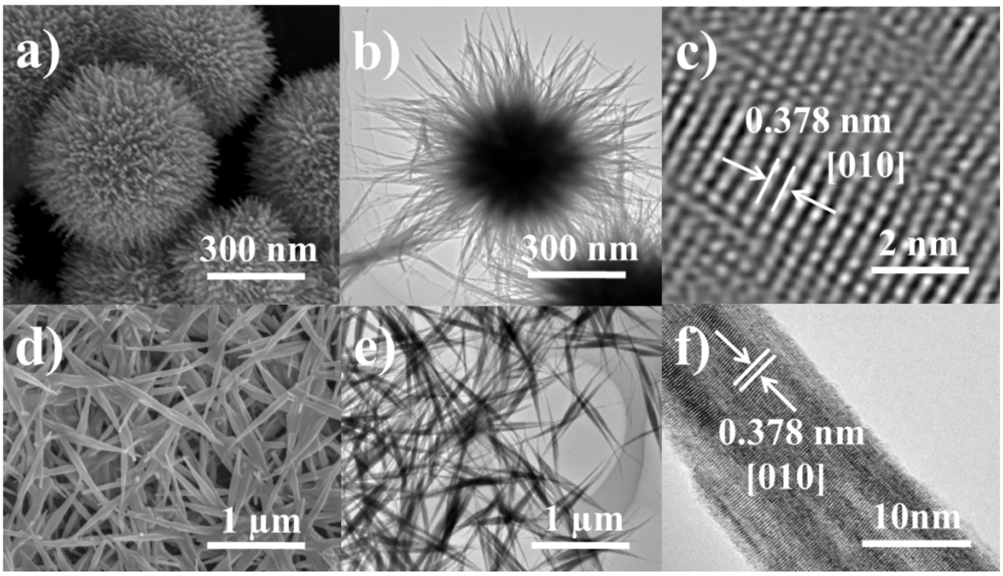

Fig. S1. (a-c) SEM, TEM and HRTEM images of UWS, and (d-f) SEM, TEM and HRTEM images of NWS.

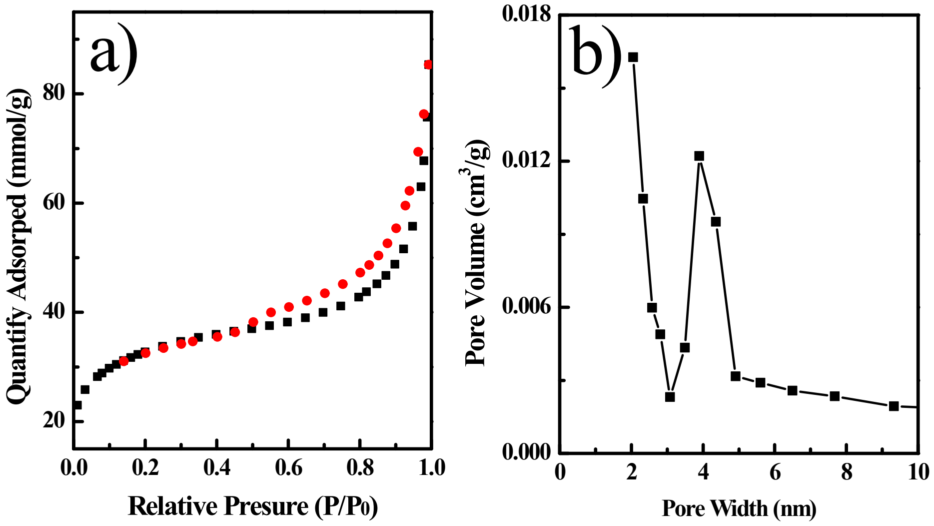

Fig. S2. (a) N_2 adsorption/desorption isotherms and (b) pore distribution of HWS.

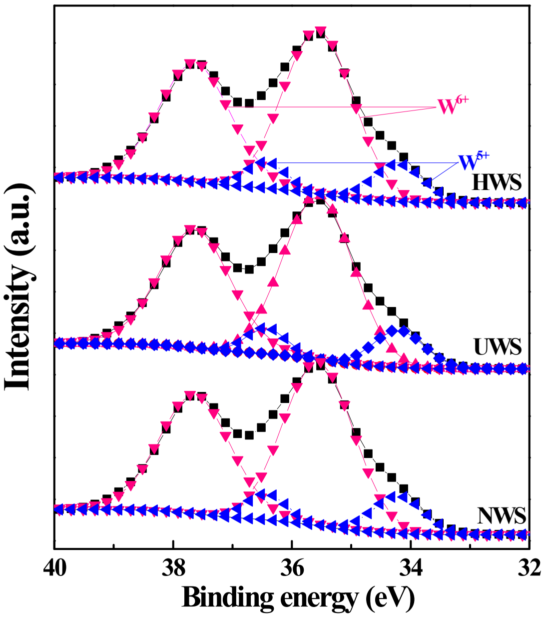

Fig. S3. W4f XPS spectra of $W_{18}O_{49}$ samples.

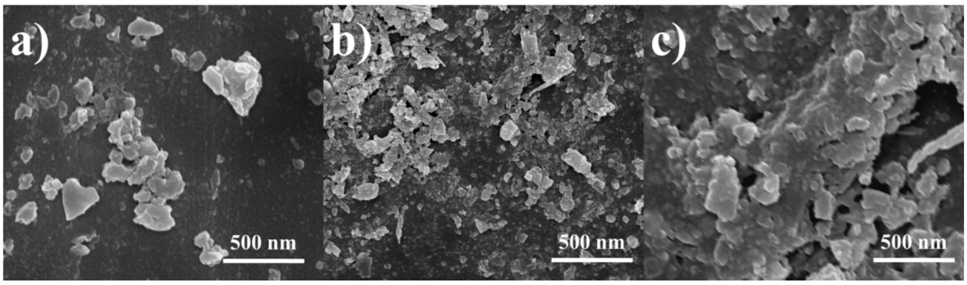

Fig. S4. SEM images of $W_{18}O_{49}$ after ball-milling. (a: HWS; b: UWS; c: NWS)

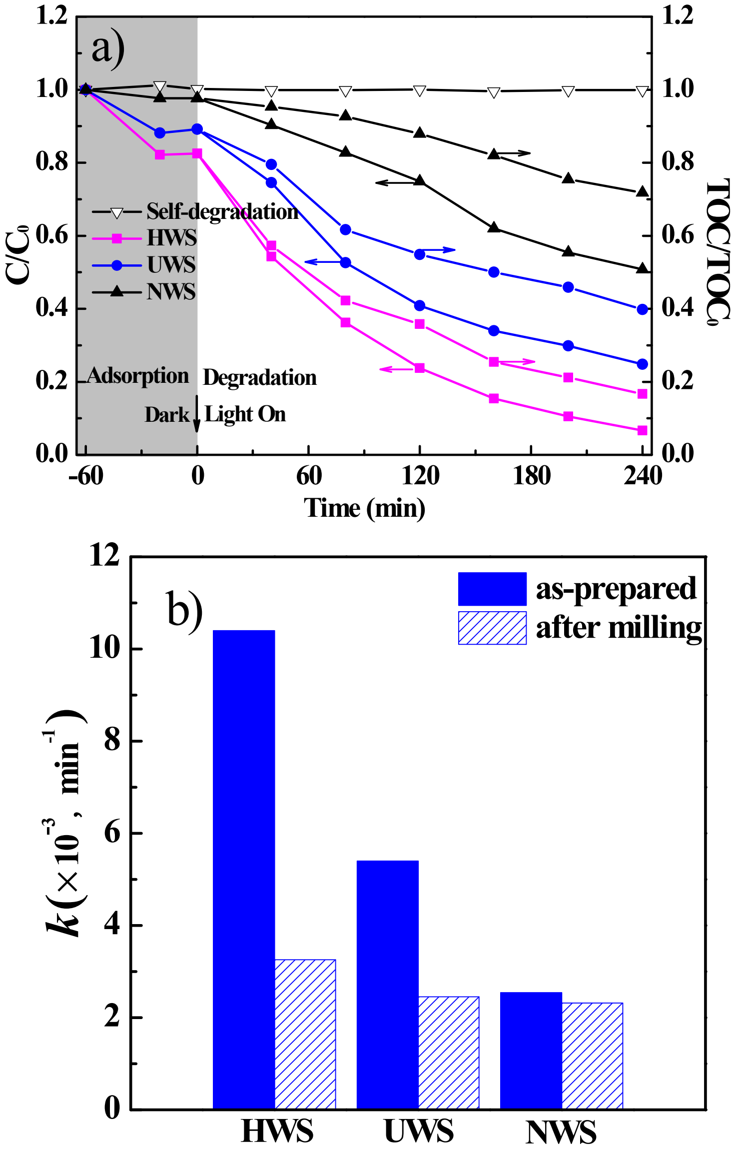

Fig. S5. (a) C/C_0 and TOC/TOC_0 as a function of irradiation time (t) for MO degradation, and (b) Photoreaction rates in degradation of MO under UV-vis light.

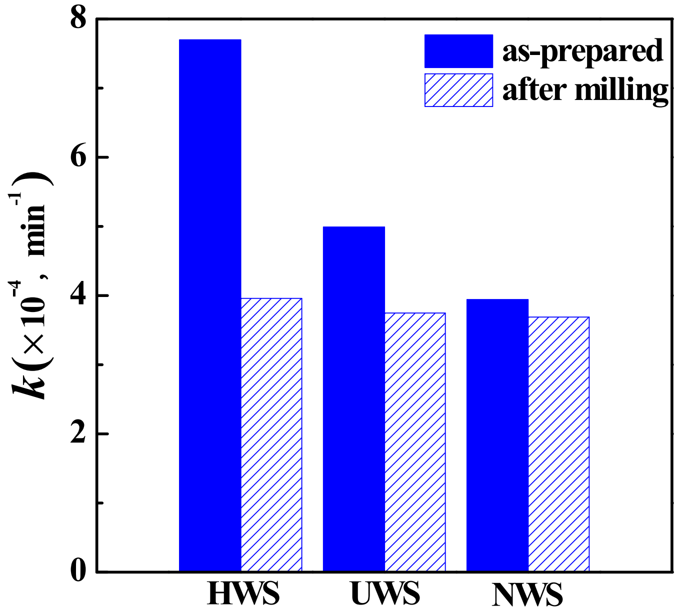

Fig. S6. Photoreaction rates in degradation of phenol under UV-vis light.

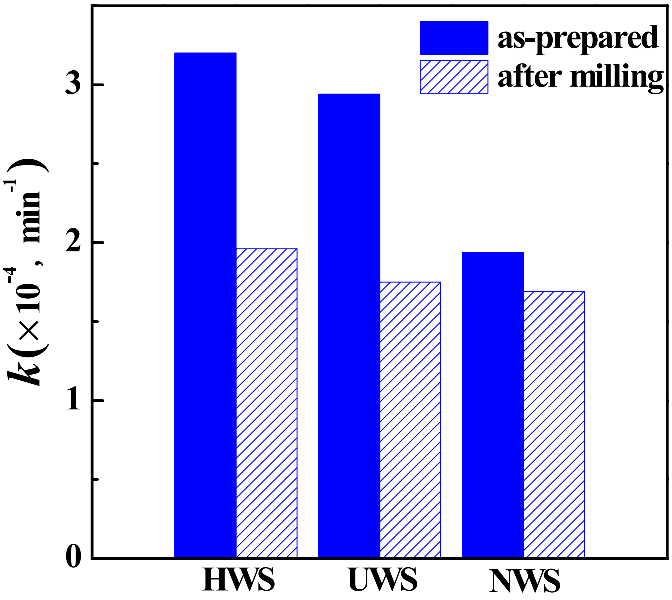

Fig. S7. Photoreaction rates before and after ball-milling in degradation of MO under visible light.

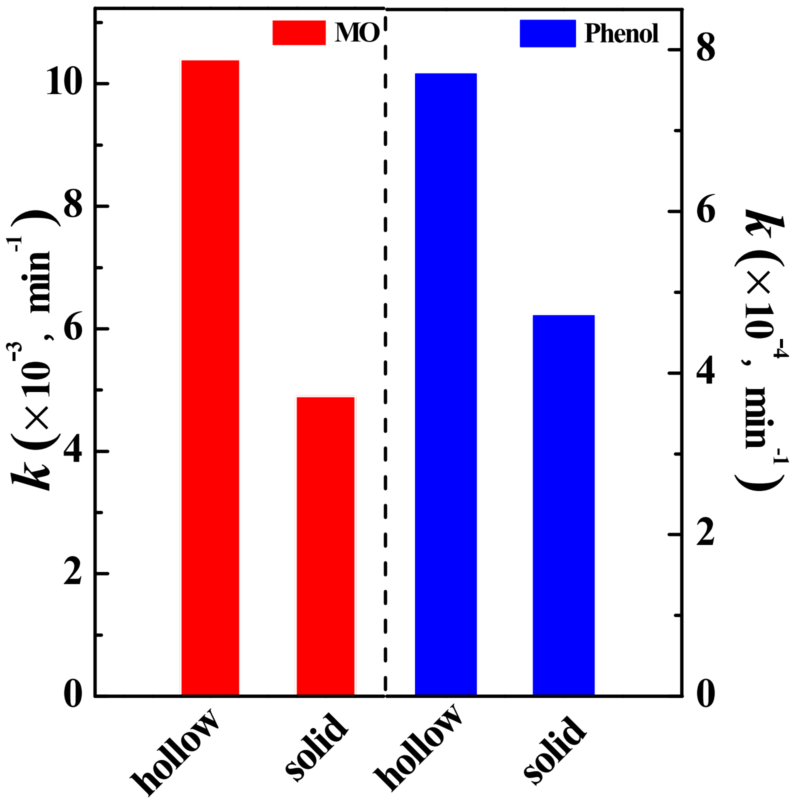

Fig. S8. Photoreaction rates of hollow and solid $W_{18}O_{49}$ spheres in degradation of MO and phenol under UV-vis light.

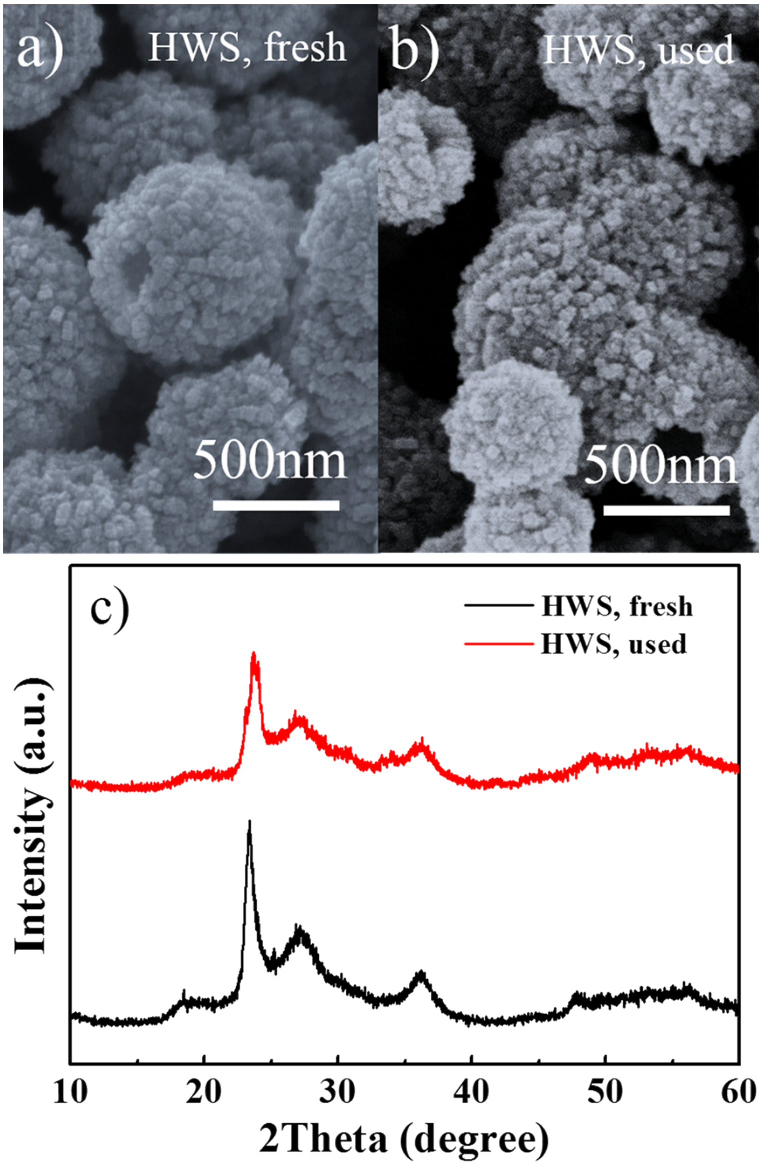

Fig. S9. (a, b) SEM images and (c) XRD patterns of HWS before and after photocatalytic reaction.

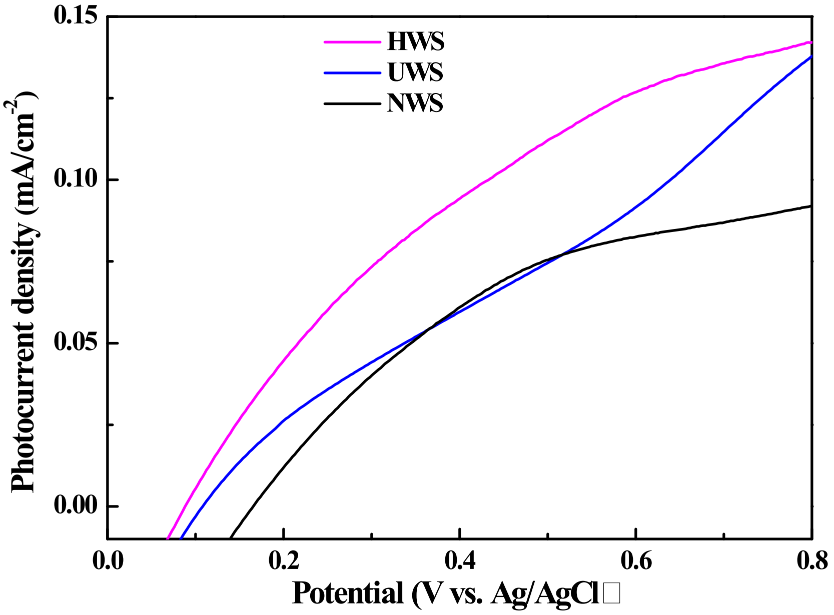

Fig. S10. Photocurrent density versus applied voltage in 0.2 M Na_2SO_4 aqueous under UV-vis irradiation.